CHINESE OPTICS LETTERS

Vol. 23, No. 1 | January 2025

Simultaneous temperature and strain sensing based on a supermode interferometer

Zhifeng Wang (王之凤), Jing Wen (文 菁), Mengshi Zhu (朱梦实), Heming Wei (魏鹤鸣), Liang Zhang (张 亮), and Fufei Pang (庞拂飞)*

Key Laboratory of Specialty Fiber Optics and Optical Access Networks, Joint International Research Laboratory of Specialty Fiber Optics and Advanced Communication, Shanghai Institute for Advanced Communication and Data Science, Shanghai University, Shanghai 200444, China

*Corresponding author: ffpang@shu.edu.cn

Received May 22, 2024 | Accepted July 18, 2024 | Posted Online February 4, 2025

A novel Mach–Zehnder interferometer (MZI) sensor based on multiple supermode interferences that can be used for dual-parameter measurements of temperature and strain is proposed and demonstrated. The MZI is made by splicing a coupled four-core sapphire-derived fiber (FSDF) between two single-mode fibers, utilizing the differences in temperature response and strain response of different supermodes in the FSDF to realize the simultaneous measurement of the two parameters. Experimental results demonstrate that the proposed MZI can achieve up to 1600 με and 1000°C measurements with a temperature-strain cross-sensitivity of approximately 0.075°C/με.

Keywords: supermode; dual-parameter measurement; fiber optic sensor; Mach-Zehnder interferometer.
DOI: 10.3788/COL202523.011202

1. Introduction

Fiber optic sensors have the advantages of compact structure, high sensitivity, and strong resistance to electromagnetic interference. They can be widely used in aerospace, petroleum, chemical, and other industrial fields for the measurement of physical parameters such as temperature, pressure, and strain[1]. Currently, commonly used fiber optic sensors include fiber Bragg gratings (FBGs)[2], Fabry–Perot interferometers (FPIs)[3], long-period fiber gratings (LPFGs)[4], and Mach–Zehnder interferometers (MZIs)[5]. However, due to the cross-sensitivity problem, it is often difficult for sensors with only a single grating structure or a single interferometric structure to achieve simultaneous measurement of dual parameters such as temperature and strain. Especially at high temperature and high strain, the discrimination of the two parameters is extremely challenging.

With regard to this problem, researchers have made various proposals[6,7]. In general, they can be divided into two main categories. One is to cascade multiple gratings or interferometers, utilizing different sensing structures that respond differently to temperature and strain, for example, cascading an LPFG and an air Fabry–Perot (FP) cavity[8], cascading two different FP cavities[9], cascading a pair of FBGs[10], cascading an FBG and an FPI[11], cascading an FBG and a MZI[12], cascading two MZIs[13], etc. Although these structures can achieve high sensitivity and high-temperature measurement, the preparation steps are relatively complex and costly. In order to fabricate a compact dual-parameter measurement sensor, another proposal of an inter-modal interference sensor containing multiple modes of interference was proposed. In 2017, Naeem *et al.* fabricated an all-fiber multibeam MZI based on two-core photonic crystal fiber[14], achieving temperature measurements up to 500°C with a sensitivity of 16.3 pm/°C and a strain range of 4000 με at room temperature with a strain sensitivity of −1.59 pm/με. In 2018, Dong *et al.* fabricated and designed a platinum (Pt)-coated MZI for simultaneous measurement of strains up to 2000 με and temperatures up to 100°C[15]. The maximum temperature sensitivity and strain sensitivity are approximately 55.2 pm/°C and −2.21 pm/με, respectively. Such an MZI has a simple structure and simple preparation steps but has not yet been able to realize strain sensing measurements in the high-temperature range.

Supermodes are transmission modes supported by coupled multicore fibers whose large mode fields make them highly sensitive to parameters such as temperature, bending, and strain[16]. At present, it has been reported that a residual stress-free, supermode interference-based Ge-doped silica fiber MZI based on supermode interference can withstand high temperatures of 1000°C with a sensitivity of up to 52 pm/°C[17] and can also achieve a strain range of 730.34 με with a sensitivity of about 16.11 pm/με[18]. Therefore, a supermode interference-based MZI has the potential to enable high-sensitivity sensing for simultaneous measurement of high temperature and strain.

In this work, we have proposed an all-fiber MZI sensor based on different supermode interferences for simultaneous temperature and strain measurements. A coupled four-core

© 2025 Chinese Optics Letters

sapphire-derived fiber (FSDF), which can support multiple supermode transmissions, was spliced with two single-mode fibers (SMFs) to fabricate the sensor. Benefiting from the high concentration of alumina doped in the core, the FSDF has advantages in high-temperature resistance and high mechanical strength. The experimental results demonstrate that an FSDF-MZI can achieve 1000°C temperature sensing and 1600 με strain sensing. At the same time, due to the different responses of short-wavelength and long-wavelength spectra to temperature and strain, a dual-parameter measurement can be realized with a temperature-strain cross-sensitivity of about 0.075°C/με. The maximum temperature sensitivity and strain sensitivity of this sensor are 61 pm/°C and 14.3 pm/με, respectively, which are higher than those of sensors that have been reported in Refs. [11,14,15,19]. Such an MZI sensor has an important application prospect in high-temperature fields such as aerospace and steel metallurgy.

2. Sensing Principle and Preparation of the FSDF-MZI

FSDF is a silica-based special fiber with four cores doped with a high concentration [about 16% (mole fraction)] of alumina, with a core diameter of approximately 3.25 μm. Figure 1(a) is the cross-sectional micrograph of the FSDF. The refractive index difference (RID) between the core and cladding is about 0.032, so each core can support four modes (LP_{01}, LP_{11}, LP_{21}, and LP_{02}). Due to the small core-to-core pitch, the field distributions of each core affect each other, resulting in new modes called supermodes. A supermode is a linear combination of the modes supported by four fiber cores, so the supermodes supported by the FSDF can be referred to as LP_{01}-like supermode (LP_{01S}), LP_{11}-like supermode (LP_{11S}), LP_{21}-like supermode (LP_{21S}), and LP_{02}-like supermode (LP_{02S}), as shown in Fig. 1(b).

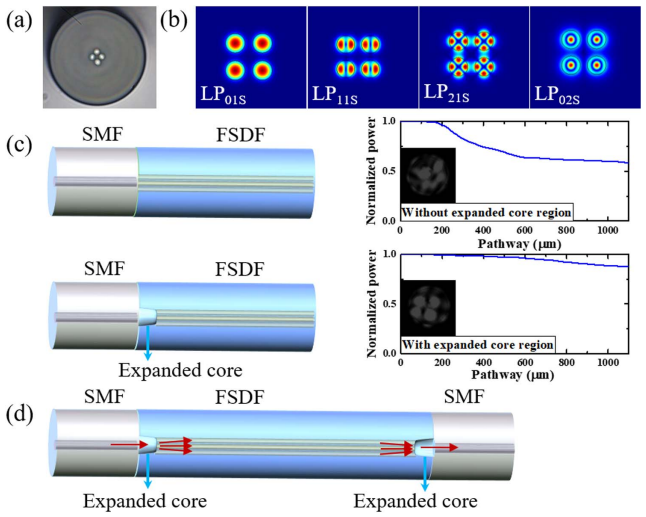

Fig. 1. (a) Cross-sectional micrograph of the FSDF. (b) Profiles of four supermodes excited in the FSDF. (c) Optical coupling in SMF into FSDF with and without the core expanded region. (d) Schematic diagram of the FSDF-MZI.

When an FSDF and an SMF are fusion spliced, the aluminum and silicon elements in the core will diffuse to the cladding. If the splicing temperature is high enough, the four cores will merge at the fusion point, forming an expanded core region with a lower refractive index (RI) from the cladding. Figure 1(c) shows the light spots of the FSDF without and with the expanded core region and simulates the change in optical power coupled from the SMF to the FSDF. It can be found that the expanded core region can evenly couple the light in the SMF into the four cores but also improves the coupling efficiency. Such an expanded core region can be used as a coupler or a beam splitter[20] so that splicing the FSDF with two SMFs can form an MZI, as shown in Fig. 1(d).

The spectrum of the supermode interference-based MZI can be expressed as[21]

$$I = \sum_{i=1}^{N} I_i + 2\sum_{i=1}^{N}\sum_{j=2}^{N}\sqrt{I_i I_j}\cos(\Delta\varphi_{ij}) \quad (i<j), \tag{1}$$

where I_i and I_j are the intensities of the guide supermodes. The subscripts i and j are integers, representing the orders of the supermodes. $\Delta\varphi_{ij}$ is the phase difference between the ith and jth mode, $\Delta\varphi_{ij} = 2\pi \cdot \Delta n_{\text{eff}} \cdot L/\lambda$, Δn_{eff} is the effective RID between supermodes, L is approximately the length of the FSDF, and λ is the wavelength. When $\Delta\varphi_{ij} = (2m+1)\pi$, m is an integer and the interference wavelength (λ_m) can be expressed as $\lambda_m = 2 \cdot \Delta n_{\text{eff}} \cdot L/(2m+1)$. The free spectral range (FSR) of the MZI is calculated with

$$\text{FSR} = |\lambda_m - \lambda_{m-1}| \approx \frac{2 \cdot \Delta n_{\text{eff}} \cdot L}{2m+1}. \tag{2}$$

Δn_{eff} between different supermodes is different, that is, the FSR of the spectra obtained by the interference of different supermodes are different. Therefore, the supermode participating in the interference can be estimated based on the FSR of the sensor.

When the FSDF-MZI sensor is subjected to an external strain (ε), not only its interference cavity length will change but also its RI will change due to the elasto-optic effect[22]. The introduced RI change (Δn) can be expressed as

$$\Delta n = -\frac{n^3}{2} \cdot [(1-\nu) \cdot p_{12} - \nu \cdot p_{11}] \cdot \varepsilon, \tag{3}$$

where p_{11} and p_{12} are the Pockels coefficients, ν is the Poisson's ratio, ε can be calculated as $\varepsilon = \Delta L/L$, and ΔL is the cavity length change. Δn can affect n_{eff} of the supermodes supported by the FSDF, thereby affecting the interference spectrum of the FSDF-MZI. According to MZI theory[23], the strain sensitivity (S_ε) of the MZI can be expressed as

$$S_\varepsilon = \lambda_\varepsilon \cdot \left[1 + \frac{1}{\Delta n_{\text{eff}}} \cdot \frac{\partial(\Delta n_{\text{eff}})}{\partial \varepsilon}\right], \tag{4}$$

where λ_ε is the working wavelength of the sensor when subjected to strain.

Similarly, when the FSDF-MZI sensor is subjected to temperature, its L and RI will also be affected by the thermo-optical effect and thermal expansion effect. The temperature sensitivity (S_T) of the MZI can be expressed as[24]

$$S_T = -\frac{\lambda_T}{\Delta n_{\text{eff}}} \cdot \frac{\partial(\Delta n_{\text{eff}})}{\partial T}, \tag{5}$$

where λ_T is the working wavelength of the sensor when subjected to temperature.

It can be found in Eqs. (4) and (5) that the strain and temperature sensitivities have nothing to do with L. However, it should be noted that the FSR of the FSDF-MZI spectrum is related to L. With the same L, the larger Δn_{eff}, the denser the spectrum. In order to obtain spectra containing different modes of interference to achieve dual parameter measurement, taking into account multiple factors such as the dispersion curve of the FSDF, the resolution of the optical spectrum analyzer (OSA), the bending insensitivity, and the length (about 5 cm) of the heating zone of the high-temperature strain experiment system, L needs to be controlled within the range of 2.45 to 3.00 cm. Figure 2(a) shows the transmission spectra of sensors with L of 2.40, 2.45, and 2.50 cm, respectively. The MZI sensors were fabricated by splicing a segment of the FSDF between two SMFs using a fusion splicer (FUJIKURA 62S), and the arc discharge intensity and duration were about 300 bits and 1000 ms, respectively. Under such discharge conditions, an expanded core region with a length of about 285 μm was generated near the fusion point of the FSDF.

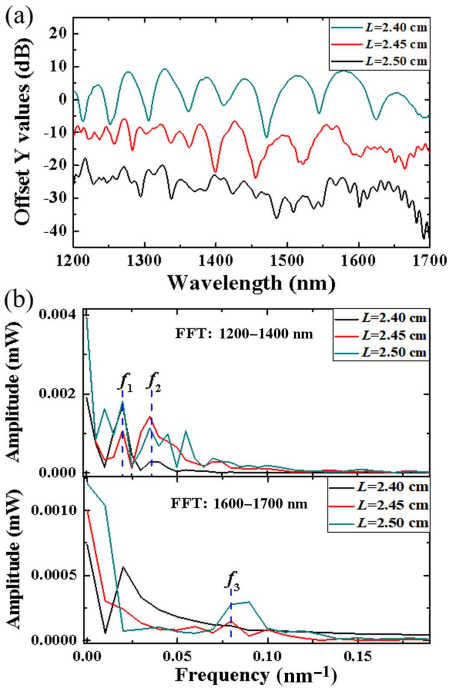

Fig. 2. (a) Transmission spectra of the FSDF-MZIs with L of 2.40, 2.45, and 2.50 cm. (b) The corresponding FFT spectra of the FSDF-MZIs: short wavelength range and long wavelength range.

It can be clearly seen from Fig. 2(a) that, when L is about 2.40 cm, the spectrum approximately only contains one frequency signal, while, when it is greater than 2.45 cm, the spectra of sensors have different FSRs in different wavelength ranges, especially in the wavelength range of 1200 to 1400 nm and 1600 to 1700 nm. This indicates that the spectra of these two wavelength ranges are obtained by different supermode interferences. To explore which modes participate in interference, we applied a fast Fourier transform (FFT) on the short- and long-wavelength ranges, as shown in Fig. 2(b). From Fig. 2(b), it can be observed that the spectrum of the sensor with L of 2.50 cm contains more frequency signals. This is because, when L is longer, the FSR corresponding to the smaller Δn_{eff} can also be obtained. Here, we mainly study the common frequency of sensors with L of 2.45 and 2.50 cm. According to the obtained three spatial frequencies, f_1, f_2, f_3, and the relationship between FSR and Δn_{eff}, it can be estimated that $\Delta n_{\text{eff1}} \approx 0.0014$, $\Delta n_{\text{eff2}} \approx 0.0024$, and $\Delta n_{\text{eff3}} \approx 0.0087$, respectively. Using the radio frequency physical field in the finite element software Comsol Multiphysics for mode analysis, n_{eff} of the supermodes supported by the FSDF can be calculated. According to the simulation results, it can be seen that the spectra with L of 2.45 and 2.50 cm from 1200 to 1400 nm is mainly obtained by $LP_{21S} - LP_{21S}$ mode interference and $LP_{02S} - LP_{02S}$ mode interference. In the long wavelength range, the spectra are mainly obtained by $LP_{01S} - LP_{11S}$ interference. This is mainly because, as the wavelength increases, higher-order modes in the core gradually cut off, and the FSDF only supports LP_{01S} and LP_{11S} transmission.

3. Strain and Temperature Measurement

Figure 3 shows the schematic diagram of the high-temperature strain measurement system of the FSDF-MZI sensor, which combines a customized tube furnace (NS-1400-18) with a universal tensile machine (SUNS UTM6000 series). The maximum working temperature of the tube furnace is 1400°C. The tensile machine is equipped with two capstans with a diameter of 50 mm for fiber fixation. The range of the force sensor is 0 to 10 N (resolution ± 0.0001 N), and the stretching speed of the tensile machine is set to 0.1 mm/min. Meanwhile, the system is equipped with a supercontinuum source (SCS, YSL SC-5) and an OSA (Yokogawa AQ6375D, resolution ± 0.2 nm) to record the spectra of the FSDF-MZI.

First, we investigated the strain-sensing characteristics of the FSDF-MZI sensor at room temperature. The distance between the two capstans is 50 cm, and the maximum displacement is set to 0.8 mm, so the tensile machine can provide a strain range from 0 to 1600 με. It can be found from Fig. 4 that the strain response of different resonant wavelengths is different. The resonant wavelength based on the $LP_{02S} - LP_{02S}$ mode interference will shift to shorter wavelengths as the strain increases, while the resonant wavelength based on the $LP_{01S} - LP_{11S}$ mode interference will shift to longer wavelengths as the strain increases.

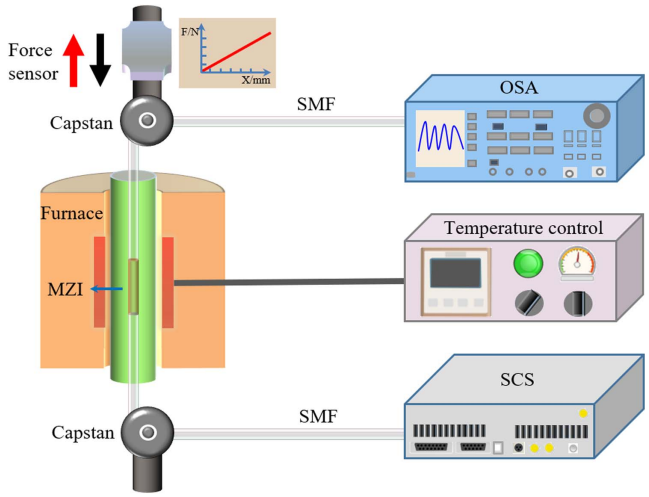

Fig. 3. Schematic diagram of a high-temperature strain measurement system for the FSDF-MZI sensor.

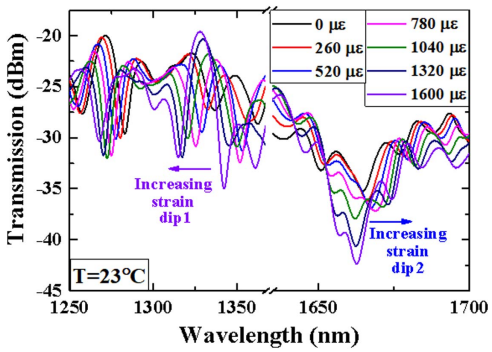

Fig. 4. Transmission spectra under different strains at room temperature.

Then we performed a round-trip tensile strain testing and tracked the shift of a wavelength [marked dip1 (1336.4 nm) and dip2 (1664.8 nm) in Fig. 4] with strain changes from the short wavelength range to the long wavelength range, respectively. The experimental results are shown in Figs. 5(a) and 5(b), respectively. The strain response of dip1 exhibits linear behavior in the range of 0 to 1600 με, with a sensitivity of approximately −14.3 pm/με, while the sensitivity of dip2 is approximately 4.6 pm/με. It is also shown that strain has a significant impact on the LP_{02S}.

We further tested the temperature characteristics and strain-sensing properties of the FSDF-MZI sensor with an L of 2.45 cm. The sensor was heated up from room temperature to 1000°C by the interval of 100°C. It was held at each temperature for 30 min for stabilization. Figure 6(a) shows the temperature characteristics of dip1 and dip2. Dip1 shifts toward shorter wavelengths with the increasing temperature, while dip2 shifts toward longer. As shown in Fig. 6(b), from room temperature to 1000°C, the temperature response of dip1 is linear, and the sensitivity of dip1 is about −25 pm/°C, while the temperature sensitivity of dip2 from room temperature to 500°C is about 22 pm/°C, and the temperature sensitivity from 500 to 800°C

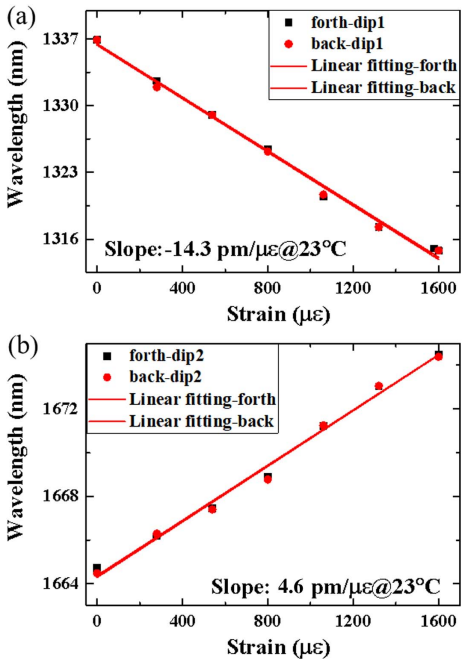

Fig. 5. Strain responses of the FSDF-MZI at room temperature: (a) dip1; (b) dip2. Forth and back represent increasing and decreasing strains, respectively.

is about 61 pm/°C. The temperature response at dip2 has a turning point at 500°C, mainly due to the release of thermal stress of the FSDF. Dip2 is the working wavelength between LP_{02S} − LP_{02S} mode interference, and thermal stress has a greater impact on it. When the sensor is sufficiently annealed, the linearity of the temperature response at dip2 will improve. The temperature characteristics of dip2 here are only monitored to 800°C because the working wavelength is about to exceed the maximum measurable range of the OSA. Dip2 itself can withstand higher temperature measurements, which we have studied before[20].

Then we tested the strain sensing property of the FSDF-MZI from room temperature to 1000°C. As shown in Fig. 6(c), the strain sensitivity of dip1 or dip2 is slightly different at different temperatures. The strain characteristics of dip2 here are only monitored to 700°C because the working wavelength is about to exceed the maximum measurable range of the OSA. We simulate the strain sensitivities of dip1 and dip2 at different temperatures by finite element software. The simulation parameters of the FSDF are set to: RID = 0.032, p_{11}, p_{12}, and v for the fiber core and cladding are referenced in Ref. [25], and the thermo-optic coefficients of the core and cladding of the FSDF are set to 0.8×10^{-5} K^{-1}[26] and 1.1×10^{-5} K^{-1}[26], respectively. Due to the dimensional error of the drawing material and the inhomogeneity of fluid convection during the fiber drawing process, the homemade FSDF is not symmetrically distributed. After further measurement with an optical microscope (BX53M, OLYMPUS), the radii (r) of the homemade FSDFs are 3.25, 3.26, 3.27, and 3.20 μm, respectively. The core–core pitches (d) are 9.0, 8.4, 8.8, and 8.0 μm, respectively. The trend of the simulated strain sensitivity from room temperature to 1000°C is generally similar to the experimental results. In addition, the strain sensitivity of

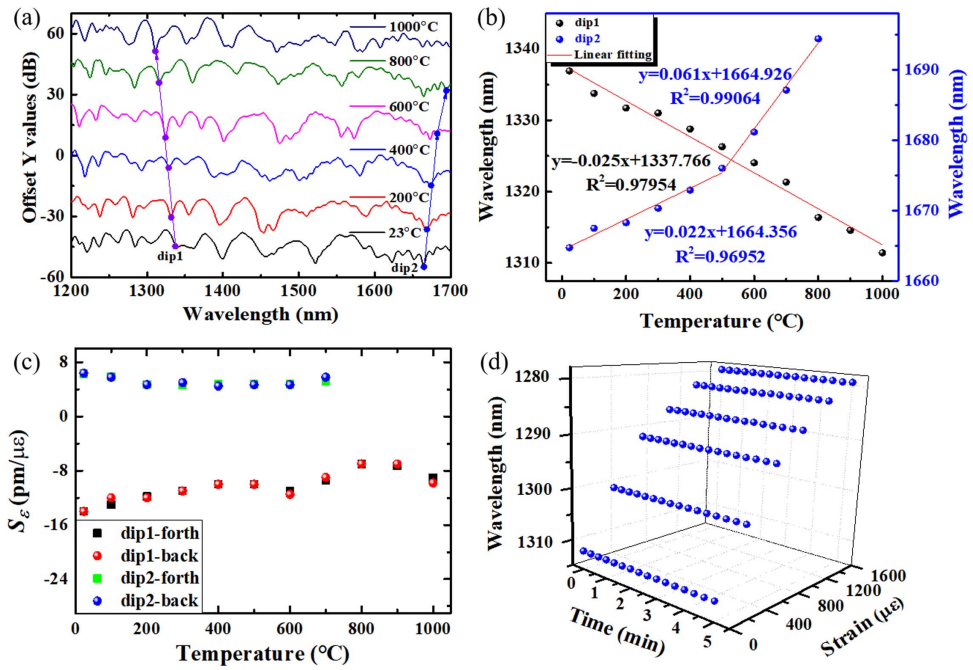

Fig. 6. (a) Transmission spectra and (b) temperature responses of dip1 and dip2 from room temperature to 1000°C. (c) Dependence of the strain sensitivities of dip1 and dip2 at different temperatures. (d) Wavelength shift versus time for each applied strain at 1000°C.

dip1 and dip2 at different temperatures when increasing strain and decreasing strain is also roughly equal, indicating that the FSDF-MZI can be used for sensor testing with a strain range of 1600 με from room temperature to 1000°C. In addition, we further investigated the strain limit of the sensor. Experimental results have shown that, when the temperature exceeds around 700°C, if a large strain (>2000 με) is applied to the sensor, the sensor is prone to fracture, mainly occurring in the SMF section. This indicates that the high-temperature mechanical strength of the FSDF is superior to SMFs.

In order to further study the stable tensile property of the FSDF-MZI sensor at 1000°C, the corresponding wavelength shift for each applied strain from 0 to 1600 με with steps of 310 με at 1000°C is measured for 5 min, as shown in Fig. 6(d). The result shows that the wavelength drift is very small under each force, and the maximum drift is about 0.08 nm, proving the stability of the FSDF-MZI sensor at 1000°C.

According to the experimental results, the developed sensor can measure temperature and strain simultaneously. For an MZI sensor, the resonance wavelength shifts of dip1 and dip2 related to temperature and strain can be obtained by the following characteristic matrix[27]:

$$\begin{bmatrix} \Delta\varepsilon \\ \Delta T \end{bmatrix} = \frac{1}{Q}\begin{bmatrix} K_{T2} & -K_{T1} \\ -K_{S2} & K_{S1} \end{bmatrix}\begin{bmatrix} \Delta\lambda_1 \\ \Delta\lambda_2 \end{bmatrix}, \tag{6}$$

where K_{T1} and K_{S1} are the temperature and strain sensitivities of dip1, respectively, K_{T2} and K_{S2} are the temperature and strain sensitivities of dip2, respectively, $\Delta\lambda_1$ and $\Delta\lambda_2$ are the shift of resonance wavelength of dip1 and dip2, respectively, Q is the determinant of the matrix, and $Q = K_{T2}K_{S1} - K_{T1}K_{S2}$. According to Eq. (6), it can be known that the thermal-induced strain sensitivity of dip1and dip2 is about 0.584 and 0.075°C/με, respectively. In addition, we also compared the

Table 1. Performance Comparison of Fiber Optic Sensors for Dual Parameter Measurement.

Type of sensor	Highest temperature sensitivity (pm/°C)	Maximum operating temperature (°C)	Highest strain sensitivity (pm/με)	Maximum strain range (με)	Cross-sensitivity (°C/με)	Reference
FBG + FPI	12.3	600	1.74	1122	0.103	[28]
MZI + FPI	72.5	800	4.24	<600	0.058	[29]
LPFG + LPFG	60.4	150	16.31	500	0.040	[30]
This paper	61.0	1000	−14.30	1600	0.075	

high-temperature and strain performance with some reported results in Table 1. The sensor we designed has certain advantages in terms of structure, high-temperature resistance, strain sensing range, sensitivity, etc.

4. Conclusion

We have demonstrated that the FSDF-MZI sensor based on multiple supermode interferences can achieve simultaneous measurement of temperature and strain. The FSDF is a core-doped alumina coupled multicore fiber that can support multiple supermode mode transmission. Benefiting from the thermal diffusion effect of the alumina-doped core in the FSDF-SMF fusion splicing process, the expanded core area not only helps to improve optical power coupling efficiency but also can be used as a coupler or beam splitter for the form of an MZI. In the experiment, we first investigated the strain-sensing characteristics of the sensor. The results indicate that the sensors based on different supermode interferences have different responses to strain. The working wavelength based on $LP_{02S} - LP_{02S}$ mode interference showed a blue shift with increasing strain, with a sensitivity of about −14.3 pm/με. The working wavelength based on $LP_{01S} - LP_{11S}$ mode interference exhibited a red shift behavior with increasing strain, and the sensitivity was about 4.6 pm/με. Taking advantage of the high-temperature resistance of the FSDF, we additionally conducted high-temperature strain performance tests on the sensor. The experimental results demonstrate that the FSDF-MZI sensor can achieve strain measurement up to 1600 με from room temperature to 1000°C. Meanwhile, due to the difference in the temperature response of $LP_{02S} - LP_{02S}$ mode interference (−25 pm/°C) and $LP_{01S} - LP_{11S}$ mode interference (61 pm/°C), since different supermodes in the FSDF have different response characteristics to temperature and strain, the FSDF-MZI can achieve simultaneous sensing of temperature and strain, with a temperature strain cross-sensitivity of approximately 0.075°C/με. The high strain and high-temperature sensing capability of the proposed sensor has attractive potential in application fields such as aerospace and steel metallurgy in the future.

Acknowledgements

This work was supported by the National Key Research and Development Program of China (No. 2023YFB3209500), the National Natural Science Foundation of China (No. U2241237), the China Postdoctoral Science Foundation (No. 2024M751934), and the Postdoctoral Fellowship Program of CPSF (No. GZC20240973).

References

1. C. K. Y. Leung, K. T. Wan, D. Inaudi, *et al.*, "Review: optical fiber sensors for civil engineering applications," Mater. Struct. **48**, 871 (2015).
2. X. Qiao, Z. Shao, W. Bao, *et al.*, "Fiber Bragg grating sensors for the oil industry," Sensors **17**, 429 (2017).
3. P. A. R. Tafulo, P. A. S. Jorge, J. L. Santos, *et al.*, "Intrinsic Fabry–Pérot cavity sensor based on etched multimode graded index fiber for strain and temperature measurement," IEEE Sens. J. **12**, 8 (2012).
4. Y. Huang, Z. Zhou, Y. N. Zhang, *et al.*, "A temperature self-compensated LPFG sensor for large strain measurements at high temperature," IEEE Trans. Instrum. Meas. **59**, 2997 (2010).
5. Y. M. Raji, H. S. Lin, S. A. Ibrahim, *et al.*, "Intensity-modulated abrupt tapered fiber Mach-Zehnder interferometer for the simultaneous sensing of temperature and curvature," Opt. Laser Technol. **86**, 8 (2016).
6. J. D. Wang, Z. Y. Wang, L. Y. Jin, *et al.*, "Dynamic large strain measurement under high-temperature environment using a modified FBG sensor and plasma surface treatment," Opt. Express **31**, 17514 (2023).
7. Z. J. Liu, L. Q. Zhu, L. D. Lu, *et al.*, "Determination of temperature and strain by a compact optical fiber Mach-Zehnder interferometer (MZI) composed of a single-mode fiber (SMF), seven core fiber (SCF), and multimode fiber (MMF) with a fiber Bragg grating (FBG)," Instrum. Sci. Technol. **49**, 457 (2021).
8. Y. J. Rao, Z. L. Ran, X. Liao, *et al.*, "Hybrid LPFG/MEFPI sensor for simultaneous measurement of high-temperature and strain," Opt. Express **15**, 14936 (2007).
9. A. Zhou, B. Y. Qin, Z. Zhu, *et al.*, "Hybrid structured fiber-optic Fabry–Perot interferometer for simultaneous measurement of strain and temperature," Opt. Lett. **39**, 5267 (2014).
10. P. Sivanesan, J. S. Sirkis, Y. Murata, *et al.*, "Optimal wavelength pair selection and accuracy analysis of dual fiber grating sensors for simultaneously measuring strain and temperature," Opt. Eng. **41**, 2456 (2002).
11. Y. J. Jiang, D. X. Yang, Y. Yuan, *et al.*, "Strain and high-temperature discrimination using a Type II fiber Bragg grating and a miniature fiber Fabry–Perot interferometer," Appl. Opt. **55**, 6341 (2016).
12. D. P. Zhou, L. Wei, W. K. Liu, *et al.*, "Simultaneous measurement for strain and temperature using fiber Bragg gratings and multimode fibers," Appl. Opt. **47**, 1668 (2008).
13. Y. J. Li, Y. F. Liu, W. H. Yuan, *et al.*, "Simultaneous measurement of axial strain and temperature based on a twin-core single-hole fiber with the optical vernier effect," Opt. Express **31**, 1705 (2023).
14. K. Naeem, I.-B. Kwon, and Y. Chung, "Multibeam interferometer using a photonic crystal fiber with two asymmetric cores for torsion, strain and temperature sensing," Sensors **17**, 132 (2017).
15. X. R. Dong, H. F. Du, X. Y. Sun, *et al.*, "Simultaneous strain and temperature sensor based on a fiber Mach-Zehnder interferometer coated with Pt by iron sputtering technology," Materials **11**, 1535 (2018).
16. X. Dong, Y. H. Xie, J. L. Ou, *et al.*, "Supermode Bragg grating inscribed in a strongly coupled seven-core fiber and its responses to temperature and curvature," Opt. Express **31**, 3258 (2023).
17. J. E. Antonio-Lopez, Z. S. Eznaveh, P. LiKamWa, *et al.*, "Multicore fiber sensor for high-temperature applications up to 1000°C," Opt. Lett. **39**, 4309 (2014).
18. L. N. Suo, Y. P. Peng, C. K. Yao, *et al.*, "High sensitivity strain sensors using four-core fibers through a corner-core excitation," Micromachines **13**, 431 (2022).
19. R. Uchimura, A. Wada, S. Tanaka, *et al.*, "Fiber Fabry-Perot interferometric sensor using Bragg gratings in polarization maintaining fiber," J. Light. Technol. **33**, 2499 (2014).
20. Z. F. Wang, H. Bartelt, Z. W. Ma, *et al.*, "Temperature sensing characteristics of a four-core sapphire derived fiber based on supermode interference," IEEE Sens. J. **22**, 19366 (2022)
21. J. N. Guan, S. J. Xu, S. Y. Liu, *et al.*, "Strain-insensitive micro torsion and temperature sensor based on a helical taper seven-core fiber structure," Opt. Express **32**, 10461 (2024).
22. M. Huang, "Stress effects on the performance of optical waveguides," Int. J. Soilds Struct. **40**, 1615 (2003).
23. J. Villatoro, O. Arrizabalaga, G. Durana, *et al.*, "Accurate strain sensing based on super-mode interference in strongly coupled multi-core optical fibres," Sci. Rep. **7**, 4451 (2017).
24. G. Coviello, V. Finazzi, J. Villatoro, *et al.*, "Thermally stabilized PCF-based sensor for temperature measurements up to 1000°C," Opt. Express **17**, 21551 (2009).
25. P. Dragic, T. Hawkins, P. Foy, *et al.*, "Sapphire-derived all-glass optical fibres," Nat. Photonics **6**, 627 (2012).

26. J. H. Wray and J. T. Neu, "Refractive index of several glasses as a function of wavelength and temperature," J. Opt. Soc. Am. B **59**, 774 (1969).
27. G. M. Zuo, W. Li, Z. Yang, *et al.*, "Double phase matching in MZI with anti-resonant effect for optical fiber sensor application," J. Light. Technol. **39**, 660 (2021).
28. C. T. Sun, C. P. Lu, X. R. Jin, *et al.*, "A new sensor for simultaneous measurement of strain and temperature," IEEE Photon. Technol. Lett. **32**, 1253 (2020).
29. H. Z. Yang, X. G. Qiao, Y. P. Wang, *et al.*, "In-fiber gratings for simultaneous monitoring temperature and strain in ultrahigh temperature," IEEE Photon. Technol. Lett. **27**, 58 (2015).
30. B. S. Huang, S. S. Xiong, Z. S. Chen, *et al.*, "In-fiber Mach-Zehnder interferometer exploiting a micro-cavity for strain and temperature simultaneous measurement," IEEE Sens. J. **19**, 5632 (2019).